Self-reporting joule heating modulated stiffness of polymeric nanocomposites for shape reconfiguration

Ji, Shaobo; Wu, Xuwei; Jiang, Ying; Wang, Ting; Liu, Zhihua; Cao, Can; Ji, Baohua; Chi, Lifeng; Li, Dechang; Chen, Xiaodong

2022

Ji, S., Wu, X., Jiang, Y., Wang, T., Liu, Z., Cao, C., Ji, B., Chi, L., Li, D. & Chen, X. (2022). Self-reporting joule heating modulated stiffness of polymeric nanocomposites for shape reconfiguration. ACS Nano, 16(10), 16833-16842. https://dx.doi.org/10.1021/acsnano.2c06682

https://hdl.handle.net/10356/167775

https://doi.org/10.1021/acsnano.2c06682

Self-reporting Joule Heating Modulated Stiffness of Polymeric Nanocomposites for Shape Reconfiguration

Shaobo Ji,[1,2] Xuwei Wu,[3] Ying Jiang,[1] Ting Wang,[1,5] Zhihua Liu,[1,4] Can Cao,[1] Baohua Ji,[3,6] Lifeng Chi,[2] Dechang Li,[3] and Xiaodong Chen[1,4]**

[1] Innovative Centre for Flexible Devices (iFLEX), Max Planck-NTU Joint Lab for Artificial Senses, School of Materials Science and Engineering, Nanyang Technological University, Singapore, 639798 Singapore

E-mail: chenxd@ntu.edu.sg

[2] Jiangsu Key Laboratory for Carbon-Based Functional Materials & Devices, Institute of Functional Nano & Soft Materials, Soochow University, Suzhou, 215123 China

[3] Key Laboratory of Soft Machines and Smart Devices of Zhejiang Province, Department of Engineering Mechanics, Zhejiang University, Hangzhou, 310027 China

E-mail: dcli@zju.edu.cn

[4] Institute of Materials Research and Engineering (IMRE), Agency for Science Technology and Research, Singapore, 138634 Singapore

[5] State Key Laboratory of Organic Electronics and Information Displays & Jiangsu Key Laboratory for Biosensors, Institute of Advanced Materials (IAM), Jiangsu National Synergetic Innovation Center for Advanced Materials (SICAM), Nanjing University of Posts and Telecommunications, Nanjing, 210023 China

[6] Oujiang Lab, Wenzhou Institute, Chinese Academy of Sciences, Wenzhou, 325001 China

ABSTRACT: Shape reconfigurable devices, *e.g.*, foldable phones, emerge with the development of flexible electronics. But their rigid frames limit the feasible shapes for the devices. To achieve freely changeable shapes yet keep the rigidity of devices for user-friendly operations, stiffness tunable materials are desired, especially under electrical control. However, current such systems are multi-layer with at least a heater layer and a structural layer, leading to complex fabrication, high cost, and loss of reprocessability. Herein, we fabricate covalent adaptable networks-carbon nanotubes (CAN-CNT) composites to realize Joule heating controlled stiffness. The nanocomposites function as stiffness tunable matrices, electric heaters, and softening sensors all by themselves. The self-reporting of softening is used to regulate the power control and the sensing mechanism is investigated by simulating the CNT-polymer chain interactions at the nano scale during the softening process. The nanocomposites not only have adjustable mechanical and thermodynamic properties but also are easy to fabricate at low cost and exhibit reprocessability and recyclability benefiting from the dynamic exchange reactions of CANs. Shape and stiffness control of flexible display systems are demonstrated with the nanocomposites as framing material, where freely reconfigurable shapes are realized to achieve convenient operation, wearing, or storage, fully exploiting their flexible potential.

KEYWORDS: stiffness control, nanocomposite, covalent adaptable network, reprocessable, self-reporting

Shape reconfigurable electronic devices, such as foldable phones, are emerging with the development of flexible electronics[1-7] and the increasing desire for both larger screens and convenient portability. Yet the existing rigid framing materials limited the possible shapes that can be accessed. Stiffness tunable materials that integrate rigidity and flexibility are thus desired to overcome the shape limitations of these devices, where the varying stiffness is to serve different purposes.[8-10] In the soft state, the devices were flexible and could be deformed to various shapes according to required application scenarios. But their softness makes them unable to hold freestanding shapes thus very inconvenient to operate. While the rigid form is to fix the desired shapes and achieve user-friendly operation in handheld or tabletop setups. The desired framing materials should keep rigid during operation and could transform to a soft state on-demand for shape-changing, and the softening is better to be sensible to regulate the stiffness tuning process. Considering the frames are for electronic devices, electricity is the most suitable stimulus for their control.

Due to the lack of electroactive materials that could change their stiffness in direct response to moderate voltage (electrorheological fluids can change their viscosity under high voltage of kV level),[11] Joule heating induced phase transition is the most used and feasible way to realize the electrically controlled stiffness. Current such systems were typically composed of several functional layers, including a structural layer, a heater layer, and a sensor layer in some cases (Figure S1A).[12-18] The multi-layer structures were complex to fabricate with high cost and the loss of reprocessability. To address these problems, especially to achieve easy fabrication and reprocessability, a single composite material that integrates all necessary functions is desired (Figure S1B).

For the composites, polymers were selected as the stiffness tunable matrix as they possess varying phase transition temperature and mechanical properties, providing sufficient selections for different requirements. Polymer phase transition based functional systems have been reported, such as triggered by photo-thermal effects or heating by additional heaters.[19-24] Electrical Joule heating of polymer itself has seldom been used due to commonly low conductivity. Current research on making conductive polymer composites was targeted in stretchable conductors where no phase transition was desired.[25-27] In those studies, conductive nanomaterials such as silver nanowires,[28-30] graphene sheets,[31-34] or carbon nanotubes (CNTs)[35-40] were physically blended with polymer substrates. Among them, CNTs, especially multi-walled CNTs, are of low cost, disperse well in polymers, and possess acceptable conductivity, thus are a good choice to endow Joule heating capability to the polymer composites.

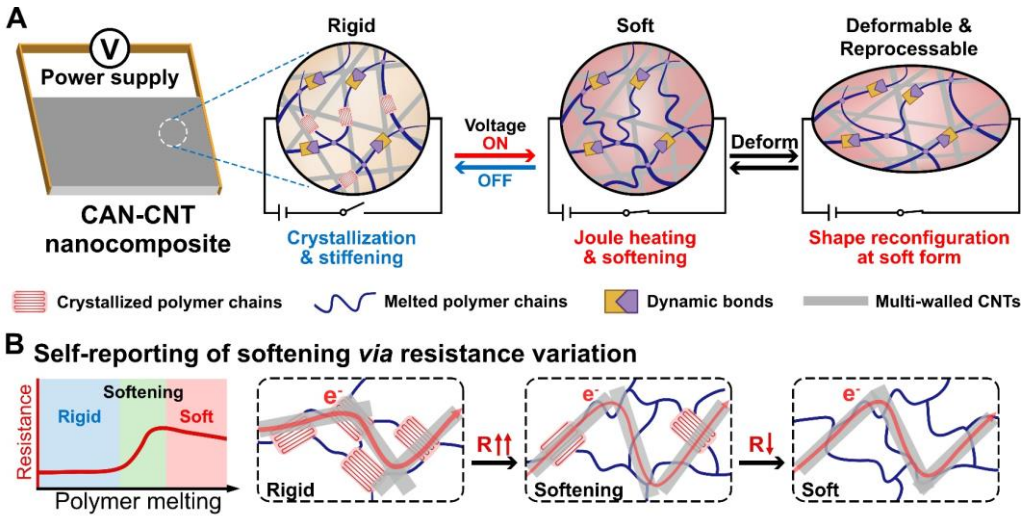

Scheme 1. Illustration of the stiffness modulation and self-reporting of softening. (A) Joule heating modulated stiffness of CAN-CNT nanocomposites. (B) The self-reporting of softening based on polymer phase transition induced polymer chain-CNT interaction variation and conductivity change.

To provide sufficient strength and keep the composite intact above the phase transition temperature, cross-linking is required (thermosets in comparison to thermoplastics). To keep reprocessability simultaneously with the strength, the cross-linked polymer can be designed as covalent adaptable networks (CANs), which are covalently cross-linked yet contain triggerable dynamic linkages for reprocessing.[19,41-47] Here, we fabricated polyurethane (PU) CAN-CNT nanocomposites to achieve electrically controlled stiffness, which required no additional units to fulfill all functions as the stiffness tunable matrix, heater, and sensor. The conductive multi-walled CNTs embedded in the nanocomposite could electrically heat the nanocomposites above their phase transition temperature to trigger rigid to soft transformation. In rigid form, the nanocomposites functioned as conventional rigid frames for shape holding and user-friendly operations, while the soft form enabled freely configurable shapes for various purposes (Scheme 1A). Unprecedentedly, the CNT-polymer chain interaction at nano scale was investigated and the peculiar resistance change during melting endowed the nanocomposite to self-report their softening (Scheme 1B). The self-reporting ability was used to regulate the stiffness control process. And the dynamic exchange reactions in CAN made it possible to reprocess and recycle the materials, which could not be achieved by previous stiffness control systems. By framing an OLED touch screen and a flexible LED array with freely reconfigurable shapes, the potential of flexible screens was better exploited.

Results and Discussion

Formula and Electrical Softening of Nanocomposites. The selection of the CAN-CNT nanocomposite was based on their properties, including the mechanical, thermodynamic, and electrical properties. The properties were determined by several parameters: structure of macromonomers, cross-linking degree, and CNT content. Polyethylene glycol (PEG4k),

hexamethylene diisocyanate (HDI), and triethanolamine (TEOHA) were used for CAN synthesis forming PU networks, in which the urethane bonds could be dynamically exchanged in the presence of catalysts at elevated temperatures (Figure 1A).[21,48-50] There are several advantages of PU-based CAN over other polymer networks: PUs are easy to synthesize with low cost and benefit large scale production for practical applications; PUs have a broad selection of main chain structures for property optimization and the combination of HDI and PEG4k provided the optimized mechanical and thermal properties with low cost; PUs with catalysts are intrinsically dynamic network and requires no further modification of the main chains to become CANs. CNT content was the most significant parameter determining the conductivity of CAN-CNT nanocomposites and was first experimented with to get the desired electrical property. With more CNT added, the conductance of nanocomposites increased (Figure 1B). For samples containing 40 %wt CNT to PEG, the conductance reached 57.0±6.2 S/m (PEG4k, 5 %wt cross-linker) at r. t. and was acceptable to function as electric heaters. When further increasing the CNT amount, there was no obvious improvement in the conductivity, but the properties became unstable (87.0±46.2 S/m, tested from 5 samples), thus 40 %wt CNT to PEG was selected. Based on the CNT content, the formula was optimized to PEG4k with 40 %wt CNT and 5 % wt cross-linker and denoted as PEG4k-40CNT (See Figure S2 for details). Compared to reported CAN-CNT composites,[51] we used common monomers and took advantage of the intrinsic dynamic property of PU network, reducing the complexity and cost of the material production, thus more beneficial for practical applications and mass production.

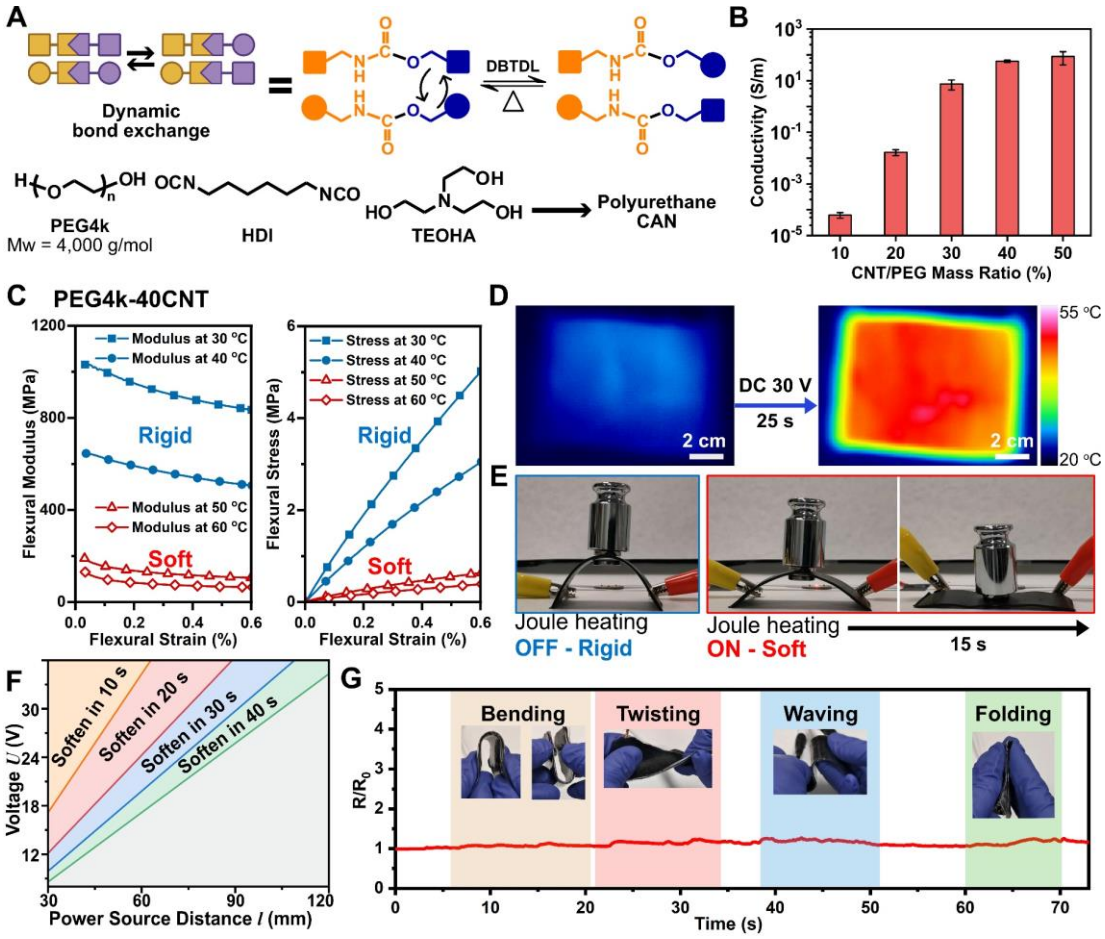

Figure 1. The Joule heating controlled stiffness change of CAN-CNT nanocomposites. (A) Dynamic exchange reactions of urethane bonds in the CAN for reprocessing and the monomers for synthesizing the CANs. (B) The conductivity of nanocomposites with varying CNT content (PEG4k, 5 %wt cross-linker). 40 %wt CNT exhibited acceptable conductivity for Joule heating and was selected for further use. (C) Flexural properties of selected CAN-CNT nanocomposite (PEG4k-40CNT) at 30 ºC, 40 ºC (rigid state) and 50 ºC, 60 ºC (soft state) showed the stiffness change and indicated that the nanocomposite could stay rigid during hand hold operations (37 ºC). (D) The function as an electrical heater of a PEG4k-40CNT plate induced uniform heating. The voltage was applied along the long side. (E) Electrically controlled softening of a PEG4k-40CNT plate. (F) Diagram of power source distance-voltage combinations for softening

(reaching 50 ºC from 30 ºC) in desired time ranges. (G) The stable resistance changes of soft state (~ 50 ºC) PEG4k-40CNT under various mechanical deformations.

The PEG4k-40CNT nanocomposite was used to demonstrate the function-integrated Joule heating modulated stiffness. The flexural modulus of PEG4k-40CNT changed from around 1 GPa to less than 100 MPa at elevated temperature (Figure 1C), exhibiting an obvious rigid/soft switch. A decrease was observed at 40 ºC but the nanocomposite was still rigid (flexural modulus > 500 MPa), indicating that it could stay in rigid form during hand hold (≤ 37 ºC) guaranteeing convenient and stable operations. Even though the stretchability was lost for the nanocomposite (Figure S3A, S3B), it was flexible in the soft state and capable to be bent for shape reconfigurations. And the flexural modulus of the rigid form (30 ºC) was at the same level as commercialized plastics under the same testing condition (Figure S3C), confirming their rigid form was strong enough to function as a free-standing framing matrix. Furthermore, PEG4k-40CNT samples were cycled of heating to soft (60 ºC) - deform - recover - cool to rigid (r. t.). The flexural modulus tested at the same bending site stayed stable after 5 cycles (Figure S3D), indicating the mechanical stability of the composite toward heating and deformation at soft state. Then the electrical heater function was tested, which was the basis of electrical control. For a 100×75×1 mm^3 nanocomposite plate, the loading of 30 V DC power along its long side could raise its temperature from r. t. (~26 ºC) to above the melting point (>45 ºC) in 25 s with homogeneous temperature distribution (Figure 1D and Movie S2). It's worth noting that for multi-layer systems, the heat was generated locally on the heater layer, which was usually patterned and would result in uneven heating of the whole system (Figure S3E) and uneven stiffness of the plates. The rigid/soft switch and Joule heating process were further combined to demonstrate the electrically controlled stiffness change. Three 9 V batteries were used in series

as power support to show their possibility to be portable. When the electrical power was off, a curved nanocomposite plate supported 100 g weight (Figure 1E). After the power was on, the plate became soft and flattened by the load, indicating the success of the electrically controlled softening process (also see Movie S3).

Joule Heating Control and Electrical Stability. The time required for Joule heating over a certain temperature range (r. t. ~30 ºC to 50 ºC for softening the nanocomposites) could be controlled by varying the power voltage U and distance l between the power connection as the setup in Figure S4A. By neglecting the change of resistance and density over the heating range (density ρ and conductivity σ were constant), the needed heating time t could be calculated as in the equation (1) (see details after Figure S4):

$$t = \frac{q\rho l^2}{\sigma U^2} = A * l^2/U^2 \quad (1)$$

where q is the heat needed per gram to increase to the target temperature, including the dissipated heat to the environment.

Though in reality the conductivity and density varied during heating, the equation could still reflect the experimental results (Figure S4B, S4C) and was enough to guide the control of heating time. From the experiment results, for the temperature range 30 ºC to 50 ºC, the constant A was 3.27 ± 0.22 $s \cdot V^2/m^2$. Thus, a power source distance-voltage combination diagram could be provided for the selection of setups with desired softening time ranges (Figure 1F).

Stable conductivity was important for repeated functions because the huge decrease in conductivity would result in the loss of electric-heating ability and stiffness control. To validate the stability, the change of conductivity with varying temperatures was first recorded. There was

an increase in the resistance when heated across the melting temperature region but didn't exceed 20 % and wouldn't hinder the Joule heating efficiency. The trend was well repeated in different samples (Figure S4D), and for the same sample, the conductivity recovered after cooling to r. t. and the curve could be repeated in subsequent heating cycles (Figure S4E). The electrical stability toward deformation at the soft state was also excellent. During various shape reconfigurations (at ~ 50 ^{o}C) such as being twisted, bent, and even folded, the resistance of the nanocomposite increased by only ~20 % (Figure 1G and Movie S4). These results indicated that the CAN-CNT nanocomposites had stable conductivity under varying temperatures and flexible shape-changing and guaranteed the possibility of multiple Joule heating-shape reconfiguration cycles.

Self-reporting of Softening and Self-regulated Power Off. The resistance-melting profile endowed the nanocomposite with the capability to self-report its softening. As shown in Figure 2A, the slope of the R/R_0-Temperature curve changed from positive to negative (resistance changed from increasing to decreasing) across the melting point, which could be used as the identifier for melting, *i.e.* softening. By simultaneously monitoring the resistance of the nanocomposites, they could function as a sensor themselves.

A regulating program was used to show their function as a sensor to self-report their softening. The threshold for triggering power off was set as a resistance drop of a certain percentage from the highest point (Figure S4F). With a lower threshold, it powered off earlier and reached a lower peak temperature (Figure 2B). The thresholds (0.1~0.3%) might seems to be tiny compared to the resistance change during deformation (Figure 1G), however, the deformation should happen at the soft state where the self-reporting was already finished. Therefore the selected thresholds were mainly based on the final temperature rather than their absolute values.

For a specific sample, when the threshold was set as 0.2% drop of resistance, the peak temperature reached above 60 °C, at which softening was achieved. The self-reporting and power-off process could be well repeated (Figure 2C). By varying the self-reporting threshold, different target peak temperatures could be regulated, showing their potential as smart materials.

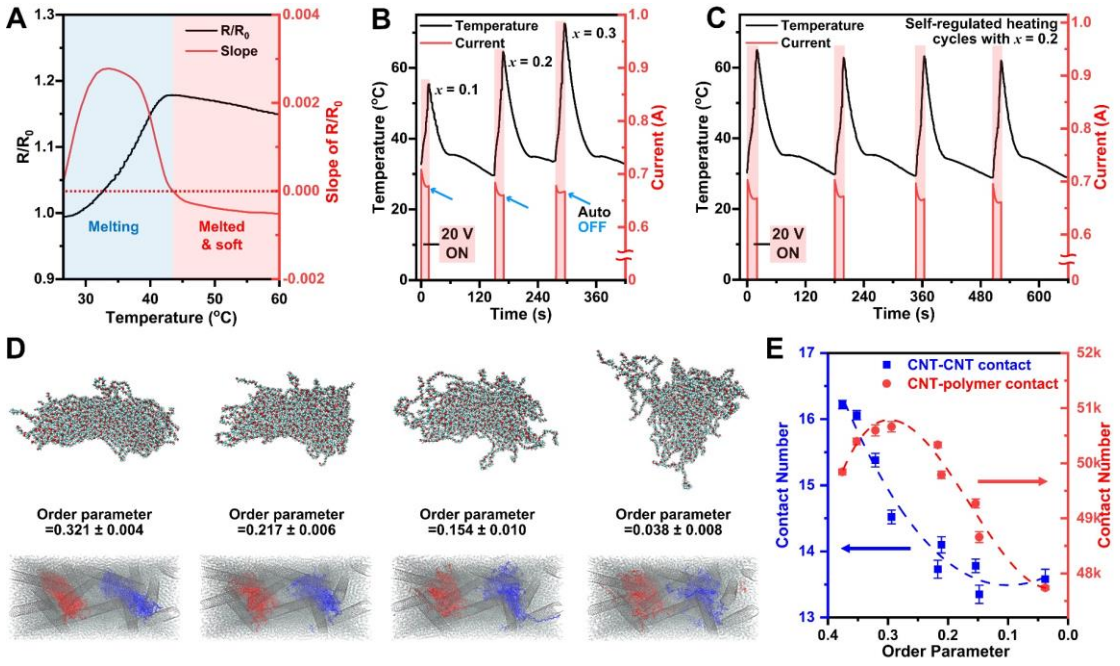

Figure 2. Self-reporting of softening and self-regulation of power. (A) The temperature-dependent change of resistance reflected the melting state and softening. The decline of resistance happened after the melting and was used as an indicator of softening. Programmed self-regulated power off when a resistance drop of x % from the highest point was detected (B) with varying threshold and (C) repeated under the same threshold. The threshold determined the peak temperature, the applied voltage was 20 V, and the electric current reflected the resistance change. (D) Simulation results of the PEG melting process of 2.7×2.7×13.8 nm^3 size crystal (above) and 2 crystals with CNTs (below, blue and red indicated 2 individual crystals). The melting resulted in decreased order parameters. (E) Simulation results of the variation of CNT-

CNT and CNT-polymer contact number (distance < 0.4 nm) with different order parameters, *i.e.* during the melting of PEG crystals.

The mechanism of the resistance-melting profile was studied through molecular dynamics simulations by GROMACS. The simulation was carried out at nano scale under different temperatures to produce the order parameter and CNT contact profiles. The order parameter indicated the melting status of the PEG crystals, with lower values, they were less crystalized (Figure 2D and Figure S5). And the CNT-CNT contact number was the most important parameter responsible for conducting electricity, the lower this value, the higher the resistance. The simulation results were shown in Figure S6, the change of CNT-CNT contact and CNT-polymer contact with changing order parameters was summarized in Figure 2G to illustrate the simulated resistance-melting relationship. With decreasing of the order parameter, the CNT-CNT contact first decreased obviously, and then became relatively stable. It indicated that the resistance first increased when melting started, and became stable after the melting process, which was consistent with the experimental results. The contact decrease was not simply due to the thermal expansion as the density of the nanocomposite still kept decreasing after melting (Figure S6A). The simulation results provided a possible explanation for this phenomenon. As shown in Figure 2E and Figure S6D, the CNT-polymer contact increased to a peak value during melting and then decreased after melting. The increase could be caused by polymer chain rearrangement during the transformation from crystal to random chains while the polymer chains were extending. The decrease could be attributed to the enhanced chain mobility with elevated temperature and the polymer chains become more dynamic rather than anchoring to the CNTs. The increased contact between CNT and polymer would induce rearrangement of CNTs and the polymer chains would block more surface area on CNTs, resulting in decreased CNT-CNT

contact. After phase transformation finished, the CNT-polymer contact number decreased and the influence of polymer chain on CNT contact became less. Meanwhile, the mobility of CNT was not affected much by the melting, eventually leading to relatively stable contacts. When the nanocomposite was recrystallized, the polymer chains tend to return to the original arrangement before melting, thus the CNT-CNT contact was also reset, and the resistance was recovered.

According to the mechanism study, the self-reporting ability was based on the typical nano filler-polymer chain interactions and resulting resistance change during polymer matrix melting[52] instead of temperature change, thus the strategy and regulating program could be directly applicable to other conductive nanomaterial-polymer nanocomposite systems regardless of their melting points and molecular structures.

Reprocessable Nanocomposite. Compared to multi-layer systems, the simple and all-function-in-one nanocomposite showed advanced processability. As mechanical processing and reshaping the nanocomposite would not damage any of the functions of the nanocomposite, it could tolerate processes such as cutting and be easily resized or reshaped. As shown in Figure 3A, PEG4k-40CNT remained functional after being cut to an 'NTU' shape and could be Joule heated. On the contrary, a multi-layer plate with a heater sandwiched between PEG4k-0CNT lost its function after cutting as the heater pattern and circuit were damaged (Figure 3B). Besides, the intended selection of polymer CANs endowed the nanocomposites with reprocessability, which could not be realized by the multi-layer systems. For the CANs without CNT, the stress relaxation under compression showed a temperature-dependent rate (Figure 3C), in accordance with reported CAN systems.[21] The CANs with CNT also showed stress relaxation phenomena under compression (Figure S7A). At the same temperature, nanocomposites with more CNT showed less relaxed stress due to the increased incompressible content, but their time for

reaching equilibrium was similar, indicating that CNT wouldn't influence much on the kinetics of dynamic exchange reactions. This made it possible to reprocess and even recycle the nanocomposites.

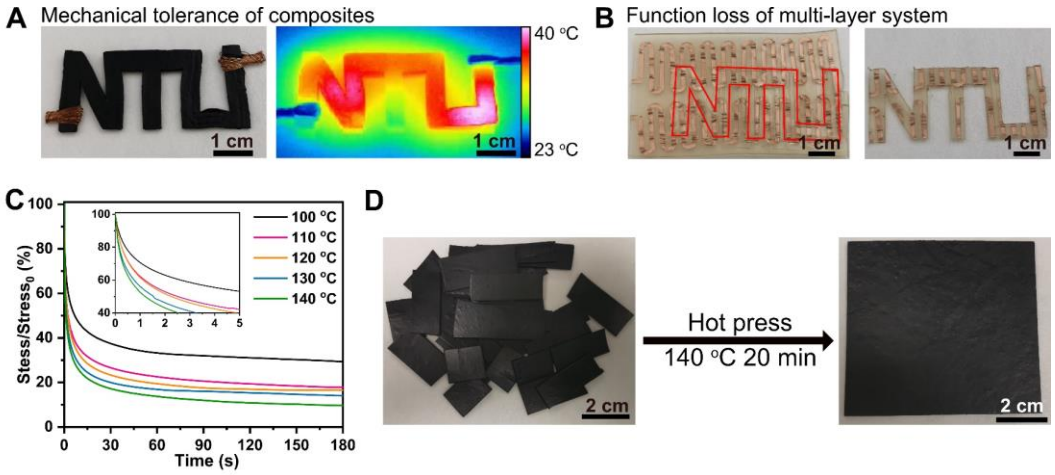

Figure 3. Mechanical tolerance and reprocessability of CAN-CNT nanocomposites. (A) The photo and IR image of a PEG4k-40CNT sample cut to an 'NTU' shape indicated its tolerance to cut and processing. (B) A multi-layer system with a 9 μm copper film heater sandwiched by two of 0.5 mm thick PEG4k-0CNT was cut to an 'NTU' shape (red frame) and lost its function as the heater layer was damaged. (C) Compression stress relaxation of PEG4k-0CNT under 0.5 strain, which showed temperature dependence in accordance with the reported CAN systems. (D) Photos of shredded PEG4k-40CNT and recycled plate *via* hot pressing.

The rigid-soft transformation also endowed the nanocomposites with shape memory effects (Figure S7B and Movie S5). Thus the reprocessability was exhibited through reconfiguring their permanent shapes. PEG4k-40CNT plates with the same pristine flat shape were reprocessed at elevated temperatures to fix new permanent shapes (Figure S7C). After changing to temporary shapes, all the samples could recover to the new permanent shapes during power ON/OFF cycles

through shape memory effects (Movie S6-8), indicating successful reprocessing with intact functions. The capability of permanent shape reconfiguration provided the possibility to repurpose and functionalize the frames even after they were produced for specific applications.

Furthermore, the nanocomposites also exhibited certain recyclability. After being cut into pieces, the nanocomposite could be hot-pressed into an intact plate at an elevated temperature (Figure 3D), and the mechanical properties could be retained (Figure S7D). However, their conductivity declined to the level of 30 %wt CNT nanocomposites after the first cycle, as the shredding had damaged the contacts between CNTs. By pressing 4 layers together (Figure S7E), the boundary of the 4 original layers was not seen in the cross-section of the pressed new plate (Figure S7F), indicating the reconnection of polymer networks.

Framing Devices for Controlled Shape Reconfiguration. To demonstrate the advantages of the electrically controlled stiffness in applications, a robust flexible LED array was framed by PEG4k-40CNT plates (Figure S8A). The LED array could function well in the soft frame state during shape-changing (Movie S9), and the rigid frame state could be configured to various free-standing patterns to fulfill different display requirements, even triangle shapes with sharp angles (Figure S9A and Movie S10). The frame also endowed the device with different operation modes (Figure 4A). It could be handheld in rigid flat mode, and when needed, it could be switched to soft form and attached to the body for wearing or ease of carrying. The fixed device with adapted curvatures would not drop off from the forearm even during fiercely shaking the arm (Movie S11), indicating excellent fixation *via* the shape adaption. The device could also be rolled up and fixed to reduce the space occupied for storage or carrying in the pocket. The introduction of stiffness tunable frames greatly expanded the possibilities of such flexible devices.

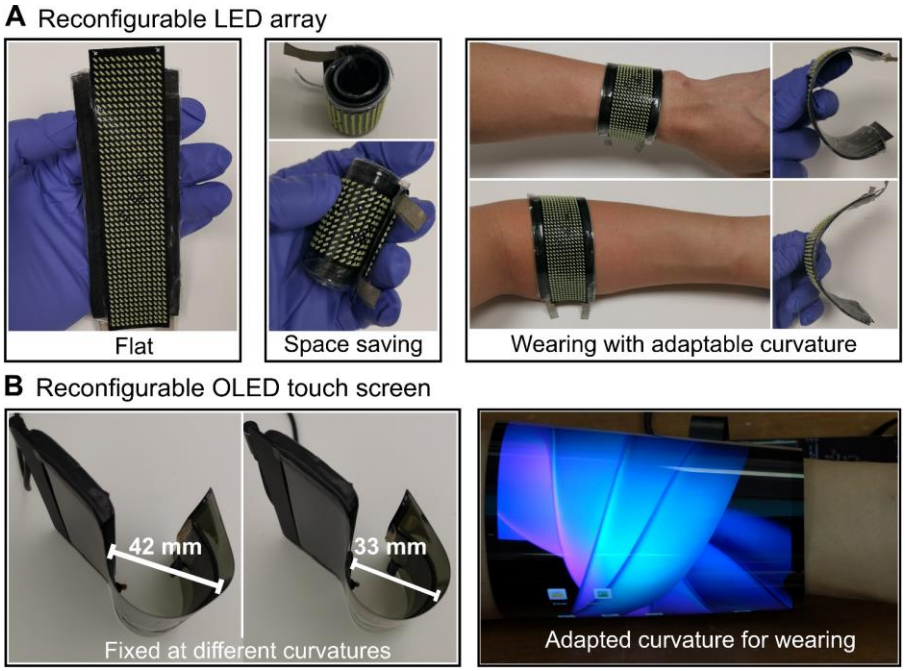

Figure 4. CAN-CNT nanocomposites supported displays with configurable shapes. (A) Mode changing/fixation of a flexible LED array, which could be fixed to different curvatures to fit different body parts and could be carried stably. (B) PEG4k-40CNT frame enabled shape reconfiguration of flexible touch screen. The screen could be shaped and fixed at different curvatures than just foldable and could be carried on desired body parts *via* controlling the curvature.

A flexible OLED touch screen was also used to further demonstrate the potential of the nanocomposites (Figure S8B). The screen could be used as normal portable devices in flat rigid mode (Figure S9B), but different from commercialized foldable devices that could only be folded along a fixed line, PEG4k-40CNT framed flexible screen possessed multiple shape configurations. At the electrically triggered soft state, the system could be flexibly deformed, and various curvatures could be realized. After switching back to the rigid state, the screen was fixed to a curved shape (Figure 4B and Figure S9C). By adapting the curvature of different body

parts, the flexible screen could function as an on-arm device, *i.e.* wearing/carrying mode, which was convenient for carrying and operations (Movie S12). Using our frames with electrically controlled stiffness, the flexible OLED screen achieved various shape reconfigurations more than simple folding yet kept all its functions, thus exploiting its potential from the flexibility and expanding its possible applications. However, currently available flexible OLED screens are still too rigid compared to our framing nanocomposite and are easily broken under high curvature, which limited their reconfigurable shapes for applications.

All the shape reconfiguration and device functions required only electricity of moderate voltage as the power source without additional units, thus of great potential for portable devices to satisfy both convenient operation and flexible shape-changing.

Conclusions

CAN-CNT nanocomposites with Joule heating modulated stiffness were designed and fabricated, which could function as the stiffness tunable matrix, heater, and softening sensor by themselves at the same time. Their mechanical and thermodynamic properties could be varied according to requirements by changing the polymer structures. Compared to multi-layer strategies, the CAN-CNT nanocomposites not only were of low cost and easy to fabricate but also inherited the reprocessability and recyclability of the CAN parts. Benefiting from the nanofillers. the nanocomposite functioned as an efficient heater under moderate voltage, *i.e.* quick softening under safe electrical control. The nanocomposites exhibited stable conductivity toward temperature change and shape variations, thus guaranteeing the repeatability of the electrically controlled process. The resistance-temperature profile, which arose from the CNT-polymer chain interactions at nano scale during melting, endowed the nanocomposite to function

as sensors to self-report the softening as well. And the potential applications of the nanocomposites in portable devices were demonstrated. A flexible OLED touch screen and a LED array were framed by our nanocomposite and could be electrically switched between rigid and soft states. The rigid state held the shape and was convenient for operation, while the soft state allowed the shape-changing to fulfill various requirements, such as carrying the device on the arm, reducing the space needed for device storage or transport, and transformation of display patterns. This polymer nanocomposite strategy to achieve electrically controlled stiffness has the advantages of versatile design, easy fabrication, low cost, reprocessability, simple setup, and safe operation conditions thus is promising for portable devices such as smartphones to realize freely shape reconfiguration rather than only foldable.

Experimental Section

Materials. Polyethylene glycol (PEG, M_w = 2000, 3000, 4000 g/mol), hexamethylene diisocyanate (HDI), dibutyltin dilaurate (DBTDL), triethanolamine (TEOHA), and chloroform (AR, contains 100 ppm amylene as the stabilizer) were purchased from Sigma Aldrich, Singapore. Multi-walled carbon nanotubes (CNT, outer diameter 30-50 nm, length 10-20 μm, –COOH functionalized) were from Timesnano, Chengdu, China. The flexible screen was a product of Royole.

Synthesis of CAN-CNT nanocomposites. Taking PEG4k-40CNT (5 %wt cross-linker) as an example, 6 g PEG4k was dissolved in 20 mL $CHCl_3$ at 60 ºC with ~120 mg DBTDL (2 %wt to PEG) added. 760 μL HDI (NCO/OH from PEG and TEOHA ratio 1.05) was added and the mixture was magnetically stirred at 60 ºC for 15 min. 300 mg TEOHA in 4 mL $CHCl_3$ was added and the mixture was further stirred for 3 min. Then the mixture was poured into a beaker

containing 2.4 g CNT wetted with 10 mL $CHCl_3$ and sonicated for 2 min while being stirred. In the end, the mixture was poured into a polytetrafluoroethylene mold (9 * 9 cm^2 square), placed on a hot plate (~45 ºC surface temperature) in a fume hood for 2 h to evaporate the solvent, left in the oven at 60 ºC for 8 h to fully cure and then in the fume hood at r. t. overnight to remove residue solvent. The above-fabricated nanocomposites were hot-pressed at 140 ºC for 20 min to get plates of the desired size. Nanocomposites of other formulas were fabricated in the same procedure with changing amounts of according reagents.

Characterization of electrical, mechanical, and thermodynamic properties. The conductivity was recorded with squared nanocomposite plates by Keithley 4200A-SCS Parameter Analyzer. Instron 5567 was used for 3-point bending tests of different cross-linker amounts, with 50 mm span and 10 mm/min speed. Thermodynamic properties were tested by TA Q10 DSC instrument (-40~100 ºC range, 10 ºC/min heating and cooling speed) and TA Q800 DMA instrument (Tensile, 0.2 % strain, 1 Hz, 30~100 ºC range 3 ºC/min heating speed). TA Q800 was also used for 3-point bending tests of the nanocomposites at different temperatures (30 and 60 ºC) and commercial plastics (30 ºC) with a 50 mm span, and 1 mm/min speed. Tensile stretching at the soft state was tested by TA Q800 at 60 ºC, controlled force mode with 1 N/min speed.

Joule heating tests. For Joule heating, a GW Instek SPS-3610 DC Power Supply was used to control input power. A Fluke Ti450 Thermal Imager was used to record the temperature change. The average temperature of the nanocomposite surfaces was used for making the curves.

Conductivity change tests. For conductivity variation with temperature change, Keithley 4200A-SCS Parameter Analyzer was used to supply 12 V power (for Joule heating) and record

the resistance (R). Fluke Ti450 Thermal Imager was used to record the temperature change (T). The R-t (time) and T-t data were correlated to make R-T curves. For conductivity changes during deformation at soft state, Keithley 4200A-SCS Parameter Analyzer was used to supply 6 V power (for keeping the temperature at the desired range) and record the resistance (R).

Compression stress relaxation. An MTS C43 Mechanical Tester with a heating module was used to carry out the tests. The samples were left on the testing platform and equilibrated for 5 min before compression. All compression tests were carried out with sample thickness ~2 mm, 0.3 mm/s speed, and 0.5 strain.

Recycle and reprocess CAN-CNT nanocomposites. For recycling PEG4k-40CNT nanocomposites, the plates were shredded and then hot-pressed at 140 ^{o}C for 20 min; or cut into 4 pieces, stacked together, and hot-pressed at 140 ^{o}C for 20 min twice as the stacked 4 layers were too thick. For permanent shape reconfiguration, the plates were first heated up above the melting point, then manually fixed to desired shapes. The fixed samples were put in a 140 ^{o}C oven for 30 min to change the permanent shapes.

Procedures for demonstrations. For the stiffness change, shape memory, and permanent shape change demonstrations, three 9V batteries were used in series as the power source, and a red LED light was connected in parallel with the nanocomposites to indicate power ON (light) or OFF (dark) state in the photos and videos. For PEG4k-40CNT framed flexible screen and LED array, three 9V batteries in series were used as the power source for frame stiffness controlling. The flexible screen needs to be plugged into a power source during operation, while a 3.7 V lithium-ion battery was used for powering the LED array.

Simulation Model buildup. For the simulation, the structure of CNT was generated by Visual Molecular Dynamics[53] with 17 nm length and 1.4 nm diameter containing 2800 carbon atoms. The PEG crystal for simulation was composed of 36 chains each containing 45 repeating units (-OCH_2CH_2-), in total 11448 atoms. The crystal structure of single-chain was from Cambridge Crystallographic Data Centre (CCDC 707050)[54] with the unit number set as 45. The PEG crystal was slowly heated from 0 K to 300 K in the simulation to get its structure at room temperature, its size was 2.7×2.7×13.8 nm^3. A simulation box of 16×32×16 nm^3 was created. 18 CNTs were first added, then 12 PEG crystals, and at last 324 random PEG single chains were added to fill the spaces and to get the same weight ratio as the synthesized nanocomposite PEG4k-40CNT.

Simulation process. GROMACS[55] was used for simulation of molecular dynamics, CHARMM36 force field[56] was used for CNTs and polymer chains. All the simulations were carried out under periodic boundary conditions of the NPT ensemble. V-rescale[57] was used to couple CNTs and polymer chains at set temperatures with a time constant of 0.5 ps, respectively. The pressure was coupled to isotropic 1 bar through Berendsen[58] coupling with a time constant of 1 ps and compressibility factor of 4.5×10^{-5}. LINCS[59] was used to limit the covalent bonds of hydrogen atoms. The time step was set as 2 ps. The cutoff radius of nonbonded interactions was set as 12 Å. PME[60] was used to calculate the long-range electrostatic interactions, the relative error accuracy for the force was 10^{-5}. The simulation was carried out under 9 temperatures, 303K, 313K, 323K, 333K, 343K, 353K, 363K, 373K, and 383K. Under each temperature, the simulation ran for 100 ns and the average data from the last 10 ns was used for plotting.

Data acquisition. The energy command in GROMACS was used to analyze the density, CNT-CNT interaction energy, and CNT-polymer interaction energy of the system under different temperatures. To quantitatively simulate the contact between CNTs, it was defined as one

contact number when carbon atoms from two different CNTs get closer than 0.4 nm, thus the average contact number per CNT was simulated. For the contact number between CNT and polymers, the distance threshold was set as 0.4 nm.

Order parameter. The order parameter[61] at the long axis of the PEG crystal could be defined as:

$$S = \frac{3}{2}\langle cos^2\theta \rangle - \frac{1}{2}$$

where θ is the angle between the long axis and molecular axis, the molecular axis was defined as the vector from O_{n-1} to O_n in the PEG chain. The order parameter of a PEG chain could be calculated as:

$$\langle S \rangle = \frac{\sum_{i=1}^{n} S(i)}{n}$$

where *n* is the number of molecular axis in the PEG chain, *S(i)* is the order parameter of number *i* molecular axis. The overall order parameter of the PEG crystal was the average of the 36 PEG chains.

ASSOCIATED CONTENT

Supporting Information.

The following files are available free of charge.

Additional polymer characterization data, electrical and Jolue heating data, detailed simulation

results, recycling results, and experimental setups. (PDF)

Movie S1. Bending test of nanocomposites with varying crosslinker. (MP4)

Movie S2-S3. Joule heating and softening of PEG4k-40CNT plates. (MP4)

Movie S4. Resistance change of PEG4k-40CNT at soft state with deformation. (MP4)

Movie S5-S8. Shape memory and reprocessing properties of PEG4k-40CNT. (MP4)

Movie S9-S11. PEG4k-40CNT framed LED array. (MP4)

Movie S12. PEG4k-40CNT framed OLED flexible screen. (MP4)

AUTHOR INFORMATION

Corresponding Author

Xiaodong Chen - Innovative Centre for Flexible Devices (iFLEX), Max Planck-NTU Joint Lab for Artificial Senses, School of Materials Science and Engineering, Nanyang Technological University, 50 Nanyang Avenue, Singapore, 639798 Singapore. Institute of Materials Research and Engineering (IMRE), Agency for Science Technology and Research, 2 Fusionopolis Way, Innovis, #08-03, Singapore, 138634 Singapore. E-mail: chenxd@ntu.edu.sg

Dechang Li - Key Laboratory of Soft Machines and Smart Devices of Zhejiang Province, Department of Engineering Mechanics, Zhejiang University, Hangzhou, 310027 China. E-mail: dcli@zju.edu.cn

Author Contributions

The manuscript was written with the contributions of all authors. All authors have given approval to the final version of the manuscript.

Notes

The authors declare no conflicts of interest.

ACKNOWLEDGMENT

The authors thank the support from the Singapore Ministry of Education (MOE2019-T2-2-022), and the National Research Foundation, Singapore (NRF) under NRF's Medium Sized Centre: Singapore Hybrid-Integrated Next-Generation μ-Electronics (SHINE) Centre funding programme. Any opinions, findings and conclusions or recommendations expressed in this article are those of the authors and do not reflect the views of National Research Foundation, Singapore (NRF).

REFERENCES

1. Kim, D. H.; Lu, N.; Ma, R.; Kim, Y. S.; Kim, R. H.; Wang, S.; Wu, J.; Won, S. M.; Tao, H.; Islam, A.; Yu, K. J.; Kim, T. I.; Chowdhury, R.; Ying, M.; Xu, L.; Li, M.; Chung, H. J.; Keum, H.; McCormick, M.; Liu, P. et al. Epidermal Electronics. *Science* **2011**, *333*, 838-843.

2. Huynh, T. P.; Haick, H. Autonomous Flexible Sensors for Health Monitoring. *Adv. Mater.* **2018**, *30*, 1802337.

3. Choi, S.; Han, S. I.; Kim, D.; Hyeon, T.; Kim, D. H. High-Performance Stretchable Conductive Nanocomposites: Materials, Processes, and Device Applications. *Chem. Soc. Rev.* **2019**, *48*, 1566-1595.

4. Gao, W.; Ota, H.; Kiriya, D.; Takei, K.; Javey, A. Flexible Electronics toward Wearable Sensing. *Acc. Chem. Res.* **2019**, *52*, 523-533.

5. Liu, K.; Jiang, Y.; Bao, Z.; Yan, X. Skin-Inspired Electronics Enabled by Supramolecular Polymeric Materials. *CCS Chem.* **2019**, *1*, 431-447.

6. Kim, D. C.; Shim, H. J.; Lee, W.; Koo, J. H.; Kim, D. H. Material-Based Approaches for the Fabrication of Stretchable Electronics. *Adv. Mater.* **2020**, *32*, 1902743.

7. Li, S.; Li, Y.; Wang, Y.; Pan, H.; Sun, J. Highly Stretchable, Elastic, Healable and Ultra-Durable Polyvinyl Alcohol-Based Ionic Conductors Capable of Safe Disposal. *CCS Chem.* **2021**, *3*, 1-26.

8. Accardo, J. V.; Kalow, J. A. Reversibly Tuning Hydrogel Stiffness through Photocontrolled Dynamic Covalent Crosslinks. *Chem. Sci.* **2018**, *9*, 5987-5993.

9. Wang, L.; Yang, Y.; Chen, Y.; Majidi, C.; Iida, F.; Askounis, E.; Pei, Q. Controllable and Reversible Tuning of Material Rigidity for Robot Applications. *Mater. Today* **2018**, *21*, 563-576.

10. Levine, D. J.; Turner, K. T.; Pikul, J. H. Materials with Electroprogrammable Stiffness. *Adv. Mater.* **2021**, *33*, 2007952.

11. Dong, Y. Z.; Seo, Y.; Choi, H. J. Recent Development of Electro-Responsive Smart Electrorheological Fluids. *Soft Matter* **2019**, *15*, 3473-3486.

12. Schubert, B. E.; Floreano, D. Variable Stiffness Material Based on Rigid Low-Melting-Point-Alloy Microstructures Embedded in Soft Poly(Dimethylsiloxane) (PDMS). *RSC Adv.* **2013**, *3*, 24671-24679.

13. Shan, W.; Lu, T.; Majidi, C. Soft-Matter Composites with Electrically Tunable Elastic Rigidity. *Smart Mater. Struct.* **2013**, *22*, 085005.

14. Tonazzini, A.; Mintchev, S.; Schubert, B.; Mazzolai, B.; Shintake, J.; Floreano, D. Variable Stiffness Fiber with Self-Healing Capability. *Adv. Mater.* **2016**, *28*, 10142-10148.

15. Van Meerbeek, I. M.; Mac Murray, B. C.; Kim, J. W.; Robinson, S. S.; Zou, P. X.; Silberstein, M. N.; Shepherd, R. F. Morphing Metal and Elastomer Bicontinuous Foams for Reversible Stiffness, Shape Memory, and Self-Healing Soft Machines. *Adv. Mater.* **2016**, *28*, 2801-2806.

16. Byun, S. H.; Sim, J. Y.; Zhou, Z.; Lee, J.; Qazi, R.; Walicki, M. C.; Parker, K. E.; Haney, M. P.; Choi, S. H.; Shon, A.; Gereau, G. B.; Bilbily, J.; Li, S.; Liu, Y.; Yeo, W. H.; McCall, J. G.; Xiao, J.; Jeong, J. W. Mechanically Transformative Electronics, Sensors, and Implantable Devices. *Sci. Adv.* **2019**, *5*, eaay0418.

17. Byun, S. H.; Kim, C. S.; Agno, K. C.; Lee, S.; Li, Z.; Cho, B. J.; Jeong, J. W. Design Strategy for Transformative Electronic System toward Rapid, Bidirectional Stiffness Tuning Using Graphene and Flexible Thermoelectric Device Interfaces. *Adv. Mater.* **2021**, *33*, 2007239.

18. Jiao, D.; Lossada, F.; Guo, J.; Skarsetz, O.; Hoenders, D.; Liu, J.; Walther, A. Electrical Switching of High-Performance Bioinspired Nanocellulose Nanocomposites. *Nat. Commun.* **2021**, *12*, 1312.

19. Pei, Z.; Yang, Y.; Chen, Q.; Terentjev, E. M.; Wei, Y.; Ji, Y. Mouldable Liquid-Crystalline Elastomer Actuators with Exchangeable Covalent Bonds. *Nat. Mater.* **2014**, *13*, 36-41.

20. Zhao, Q.; Zou, W.; Luo, Y.; Xie, T. Shape Memory Polymer Network with Thermally Distinct Elasticity and Plasticity. *Sci. Adv.* **2016**, *2*, 1501297.

21. Zheng, N.; Fang, Z.; Zou, W.; Zhao, Q.; Xie, T. Thermoset Shape-Memory Polyurethane with Intrinsic Plasticity Enabled by Transcarbamoylation. *Angew. Chem. Int. Ed.* **2016**, *55*, 11421-11425.

22. Yang, H.; Leow, W. R.; Wang, T.; Wang, J.; Yu, J.; He, K.; Qi, D.; Wan, C.; Chen, X. 3D Printed Photoresponsive Devices Based on Shape Memory Composites. *Adv. Mater.* **2017**, *29*, 1701627.

23. Zhang, Y.; Zheng, N.; Cao, Y.; Wang, F.; Wang, P.; Ma, Y.; Lu, B.; Hou, G.; Fang, Z.; Liang, Z.; Yue, M.; Li, Y.; Chen, Y.; Fu, J.; Wu, J.; Xie, T.; Feng, X. Climbing-Inspired Twining Electrodes Using Shape Memory for Peripheral Nerve Stimulation and Recording. *Sci. Adv.* **2019**, *5*, eaaw1066.

24. Nonoyama, T.; Lee, Y. W.; Ota, K.; Fujioka, K.; Hong, W.; Gong, J. P. Instant Thermal Switching from Soft Hydrogel to Rigid Plastics Inspired by Thermophile Proteins. *Adv. Mater.* **2020**, *32*, 1905878.

25. Chen, J.; Yu, Q.; Cui, X.; Dong, M.; Zhang, J.; Wang, C.; Fan, J.; Zhu, Y.; Guo, Z. An Overview of Stretchable Strain Sensors from Conductive Polymer Nanocomposites. *J. Mater. Chem. C* **2019**, *7*, 11710-11730.

26. Wang, H.; Yao, Y.; He, Z.; Rao, W.; Hu, L.; Chen, S.; Lin, J.; Gao, J.; Zhang, P.; Sun, X.; Wang, X.; Cui, Y.; Wang, Q.; Dong, S.; Chen, G.; Liu, J. A Highly Stretchable Liquid Metal Polymer as Reversible Transitional Insulator and Conductor. *Adv. Mater.* **2019**, *31*, 1901337.

27. Peng, S.; Yu, Y.; Wu, S.; Wang, C. H. Conductive Polymer Nanocomposites for Stretchable Electronics: Material Selection, Design, and Applications. *ACS Appl. Mater. Interfaces* **2021**, *13*, 43831-43854.

28. Liang, J.; Tong, K.; Pei, Q. A Water-Based Silver-Nanowire Screen-Print Ink for the Fabrication of Stretchable Conductors and Wearable Thin-Film Transistors. *Adv. Mater.* **2016**, *28*, 5986-5996.

29. Cheng, Y.; Wang, R.; Sun, J.; Gao, L. Highly Conductive and Ultrastretchable Electric Circuits from Covered Yarns and Silver Nanowires. *ACS Nano* **2015**, *9*, 3887-3895.

30. Choi, S.; Han, S. I.; Jung, D.; Hwang, H. J.; Lim, C.; Bae, S.; Park, O. K.; Tschabrunn, C. M.; Lee, M.; Bae, S. Y.; Yu, J. W.; Ryu, J. H.; Lee, S. W.; Park, K.; Kang, P. M.; Lee, W. B.; Nezafat, R.; Hyeon, T.; Kim, D. H. Highly Conductive, Stretchable and Biocompatible Ag-Au Core-Sheath Nanowire Composite for Wearable and Implantable Bioelectronics. *Nat. Nanotechnol.* **2018**, *13*, 1048-1056.

31. Wang, M.; Duan, X.; Xu, Y.; Duan, X. Functional Three-Dimensional Graphene/Polymer Composites. *ACS Nano* **2016**, *10*, 7231-7247.

32. Xu, Z.; Liu, Z.; Sun, H.; Gao, C. Highly Electrically Conductive Ag-Doped Graphene Fibers as Stretchable Conductors. *Adv. Mater.* **2013**, *25*, 3249-3253.

33. Liu, N.; Chortos, A.; Lei, T.; Jin, L.; Kim, T. R.; Bae, W. G.; Zhu, C.; Wang, S.; Pfattner, R.; Chen, X.; Sinclair, R.; Bao, Z. Ultratransparent and Stretchable Graphene Electrodes. *Sci. Adv.* **2017**, *3*, 1700159.

34. Ge, J.; Zhu, H.-W.; Yang, Y.; Xie, Y.; Wang, G.; Huang, J.; Shi, L.-A.; Schmidt, O. G.; Yu, S.-H. A General and Programmable Synthesis of Graphene-Based Composite Aerogels by a Melamine-Sponge-Templated Hydrothermal Process. *CCS Chem.* **2020**, *2*, 1-12.

35. Sekitani, T.; Noguchi, Y.; Hata, K.; Fukushima, T.; Aida, T.; Someya, T. A Rubberlike Stretchable Active Matrix Using Elastic Conductors. *Science* **2008**, *321*, 1468-1472.

36. Sekitani, T.; Nakajima, H.; Maeda, H.; Fukushima, T.; Aida, T.; Hata, K.; Someya, T. Stretchable Active-Matrix Organic Light-Emitting Diode Display Using Printable Elastic Conductors. *Nat. Mater.* **2009**, *8*, 494-499.

37. Zhang, S.; Ma, Y.; Suresh, L.; Hao, A.; Bick, M.; Tan, S. C.; Chen, J. Carbon Nanotube Reinforced Strong Carbon Matrix Composites. *ACS Nano* **2020**, *14*, 9282-9319.

38. Wu, Y.; Zhao, X.; Shang, Y.; Chang, S.; Dai, L.; Cao, A. Application-Driven Carbon Nanotube Functional Materials. *ACS Nano* **2021**, *15*, 7946-7974.

39. Lin, M.; Zheng, Z.; Yang, L.; Luo, M.; Fu, L.; Lin, B.; Xu, C. A High-Performance, Sensitive, Wearable Multifunctional Sensor Based on Rubber/CNT for Human Motion and Skin Temperature Detection. *Adv. Mater.* **2021**, *33*, 2107309.

40. Liu, Z.; Wang, X.; Wei, S.; Lv, H.; Zhou, J.; Peng, P.; Wang, H.; Chen, G. A Wavy-Structured Highly Stretchable Thermoelectric Generator with Stable Energy Output and Self-Rescuing Capability. *CCS Chem.* **2021**, *3*, 2404-2414.

41. Rottger, M.; Domenech, T.; van der Weegen, R.; Breuillac, A.; Nicolay, R.; Leibler, L. High-Performance Vitrimers from Commodity Thermoplastics through Dioxaborolane Metathesis. *Science* **2017**, *356*, 62-65.

42. Delahaye, M.; Winne, J. M.; Du Prez, F. E. Internal Catalysis in Covalent Adaptable Networks: Phthalate Monoester Transesterification as a Versatile Dynamic Cross-Linking Chemistry. *J. Am. Chem. Soc.* **2019**, *141*, 15277-15287.

43. Winne, J. M.; Leibler, L.; Du Prez, F. E. Dynamic Covalent Chemistry in Polymer Networks: A Mechanistic Perspective. *Polym. Chem.* **2019**, *10*, 6091-6108.

44. Fan, C.-J.; Wen, Z.-B.; Xu, Z.-Y.; Xiao, Y.; Wu, D.; Yang, K.-K.; Wang, Y.-Z. Adaptable Strategy to Fabricate Self-Healable and Reprocessable Poly(Thiourethane-Urethane) Elastomers Via Reversible Thiol–Isocyanate Click Chemistry. *Macromolecules* **2020**, *53*, 4284-4293.

45. Patel, T.; Kim, M. P.; Park, J.; Lee, T. H.; Nellepalli, P.; Noh, S. M.; Jung, H. W.; Ko, H.; Oh, J. K. Self-Healable Reprocessable Triboelectric Nanogenerators Fabricated with Vitrimeric Poly(Hindered Urea) Networks. *ACS Nano* **2020**, *14*, 11442-11451.

46. Podgorski, M.; Fairbanks, B. D.; Kirkpatrick, B. E.; McBride, M.; Martinez, A.; Dobson, A.; Bongiardina, N. J.; Bowman, C. N. Toward Stimuli-Responsive Dynamic Thermosets through Continuous Development and Improvements in Covalent Adaptable Networks (CANs). *Adv. Mater.* **2020**, *32*, 1906876.

47. Lossada, F.; Jiao, D.; Hoenders, D.; Walther, A. Recyclable and Light-Adaptive Vitrimer-Based Nacre-Mimetic Nanocomposites. *ACS Nano* **2021**, *15*, 5043-5055.

48. Fortman, D. J.; Sheppard, D. T.; Dichtel, W. R. Reprocessing Cross-Linked Polyurethanes by Catalyzing Carbamate Exchange. *Macromolecules* **2019**, *52*, 6330-6335.

49. Elizalde, F.; Aguirresarobe, R. H.; Gonzalez, A.; Sardon, H. Dynamic Polyurethane Thermosets: Tuning Associative/Dissociative Behavior by Catalyst Selection. *Polym. Chem.* **2020**, *11*, 5386-5396.

50. Sheppard, D. T.; Jin, K.; Hamachi, L. S.; Dean, W.; Fortman, D. J.; Ellison, C. J.; Dichtel, W. R. Reprocessing Postconsumer Polyurethane Foam Using Carbamate Exchange Catalysis and Twin-Screw Extrusion. *ACS Cent. Sci.* **2020**, *6*, 921-927.

51. Orozco, F.; Kaveh, M.; Santosa, D. S.; Lima, G. M. R.; Gomes, D. R.; Pei, Y.; Araya-Hermosilla, R.; Moreno-Villoslada, I.; Picchioni, F.; Bose, R. K. Electroactive Self-Healing Shape Memory Polymer Composites Based on Diels-Alder Chemistry. *ACS Appl. Polym. Mater.* **2021**, *3*, 6147−6156.

52. He, X. J.; Du, J. H.; Ying, Z.; Cheng, H. M.; He, X. J. Positive Temperature Coefficient Effect in Multiwalled Carbon Nanotube/High-Density Polyethylene Composites. *Appl. Phys. Lett.* **2005**, *86*, 062112.

53. Humphrey, W.; Dalke, A.; Schulten, K. VMD: Visual Molecular Dynamics. *J. Mol. Graph.* **1996**, *14*, 33-38.

54. French, A. C.; Thompson, A. L.; Davis, B. G. High-Purity Discrete Peg-Oligomer Crystals Allow Structural Insight. *Angew. Chem. Int. Ed.* **2009**, *48*, 1248-1252.

55. Abraham, M. J.; Murtola, T.; Schulz, R.; Páll, S.; Smith, J. C.; Hess, B.; Lindahl, E. GROMACS: High Performance Molecular Simulations through Multi-Level Parallelism from Laptops to Supercomputers. *SoftwareX* **2015**, *1-2*, 19-25.

56. Huang, J.; MacKerell, A. D., Jr. CHARMM36 All-Atom Additive Protein Force Field: Validation Based on Comparison to NMR Data. *J. Comput. Chem.* **2013,** *34*, 2135-2145.

57. Bussi, G.; Donadio, D.; Parrinello, M. Canonical Sampling through Velocity Rescaling. *J. Chem. Phys.* **2007**, *126*, 014101.

58. Berendsen, H. J. C.; Postma, J. P. M.; van Gunsteren, W. F.; DiNola, A.; Haak, J. R. Molecular Dynamics with Coupling to an External Bath. *J. Chem. Phys.* **1984**, *81*, 3684-3690.

59. Hess, B. P-LINCS: A Parallel Linear Constraint Solver for Molecular Simulation. *J. Chem. Theory Comput.* **2008**, *4*, 116-122.

60. Essmann, U.; Perera, L.; Berkowitz, M. L.; Darden, T.; Lee, H.; Pedersen, L. G. A Smooth Particle Mesh Ewald Method. *J. Chem. Phys.* **1995**, *103*, 8577-8593.

61. Gupta, R.; Dwadasi, B. S.; Rai, B.; Mitragotri, S. Effect of Chemical Permeation Enhancers on Skin Permeability: In Silico Screening Using Molecular Dynamics Simulations. *Sci. Rep.* **2019**, *9*, 1456.

Table of content